Available online at www.sciencedirect.com
SCIENCE DIRECT®

Journal of the European Ceramic Society 24 (2004) 3453–3463
www.elsevier.com/locate/jeurceramsoc

A comparison of the microstructure and mechanical properties of two liquid phase sintered aluminas containing different molar ratios of calcia–silica sintering additives

Peter Svancarek[a,b], Dusan Galusek[a], Clair Calvert[b], Fiona Loughran[b], Andy Brown[b], Rik Brydson[b,*], Frank Riley[b]

[a]*Institute of Inorganic Chemistry, Slovak Academy of Sciences, Dúbravská cesta 9, SK-84236 Bratislava, Slovak Republic*
[b]*Institute for Materials Research, School of Process, Environmental and Materials Engineering, University of Leeds, Leeds LS2 9JT, UK*

Abstract

The microstructures of two dense polycrystalline aluminas hot pressed with a total of 5 wt.% of liquid phase-forming sintering additives: calcium oxide (CaO) and silicon oxide (SiO_2) but with differing $CaO:SiO_2$ molar ratios, have been studied using analytical scanning electron microscopy (SEM) and transmission electron microscopy (TEM) combined with energy dispersive X-ray (EDX) spectrometry and electron energy loss spectrometry (EELS). These techniques allowed the direct imaging of secondary crystalline phases and amorphous films at grain boundaries and at triple pockets as well as both a qualitative and semi-quantitative determination of their composition and chemistry. Two samples CS5 and CSp, containing $CaO:SiO_2$ molar ratios of 1:5 and 1:1.33 respectively, were studied in detail. SEM revealed big differences in median grain size between the CS5 sample, 0.56 μm, and the CSp sample, which was more than 2 times larger. TEM revealed that the CS5 sample exhibited a significant proportion of a secondary crystalline anorthite phase at triple pockets which resulted in a silica-rich glassy intergranular phase deficient in calcium possessing a composition lying in the mullite phase field of the ternary phase diagram. Conversely the CSp specimen possessed a heterogeneous glassy film which differed in composition between grain boundaries (where significant Ca was observed) and triple pockets (which were more silica-rich). The microstructure of CSp also showed evidence for dislocation arrays, strain and microcracks possibly due to the mismatch in thermal expansion coefficients between alumina grains, glassy and secondary and crystallised phases which, together with bigger grain size, may explain the reduced wear resistance relative to CS5.

Keywords: Al_2O_3; Electron microscopy; Mechanical properties; Microstructure; Wear

1. Introduction

In recent years the importance of microstructure and, in particular, grain boundary microstructure for mechanical properties in polycrystalline ceramic materials has become increasingly evident.[1] Many macroscopic properties appear to be controlled by the detailed microstructure and chemistry of grain boundaries and interfaces; examples include mechanical properties, particularly fracture processes which may be either inter- or intragranular, and electrical conductivity. Grain boundaries in ceramics generally act as a sink for insoluble impurities or processing additives and often form thin amorphous films of nanometre dimension which are remnants of the liquid phases formed during processing. The development of high spatial resolution analysis techniques within the TEM allows for the direct imaging of grain boundaries and grain boundary films and for the spectroscopic determination of their composition and chemistry, and TEM has revealed many interesting (and perhaps universal) features in polycrystalline ceramics based on silicon nitride,[2] zinc oxide varistors [3] and, in recent work at Leeds, alumina ceramics.[4]

The major characteristics that are beneficial for the wear performance of alumina ceramic materials are their high resistance to thermal shock failure, high hardness, relatively good fracture toughness and high resistance to oxidation, the latter being especially important in high temperature applications. Pure alumina ceramics are often modified by the addition of silica, calcia and other sintering additives which form liquid phases during the sintering process. These additives promote sintering and

* Corresponding author.
E-mail address: mtlrmdb@leeds.ac.uk (R. Brydson).

0955-2219/$ - see front matter © 2003 Elsevier Ltd. All rights reserved.
doi:10.1016/j.jeurceramsoc.2003.10.032

accelerate densification, via the formation of a low melting point eutectic, and their residual presence in the final microstructure can change the mechanical properties of the polycrystalline alumina considerably. Therefore the optimization of the composition and amount of additive, and hence the resultant glassy phases, are essential for the further improvement of mechanical properties of the final material. Alumina ceramics are often used as materials for cutting tools principally because of their chemical compatibility with, for example, iron and ferro-alloys where there is no possibility to use silicon nitride because of the reaction of nitrogen from the cutting tool with iron. For such applications it is essential to achieve the highest possible wear resistance and, in order to maximize this property, it is necessary to prevent alumina grain pull-out via optimization of the composition of intergranular phases.

Using silica as a sintering additive can significantly improve the wear resistance of alumina.[7] Different amounts of magnesia[5,6] and calcia[4,7] are also used to obtain intergranular silicate glasses with differing molar ratios of silica/magnesia or silica/calcia. A comparison of the properties of some of these materials is shown in Table 1 where the data has been extracted from a number of our previous studies.[4–7] Grain growth experiments have shown that ceramic samples with larger grain sizes have larger wear rates[6,8] and, for pure alumina, grain detachment was found to be the dominant wear mechanism for grain sizes > 1 μm (i.e. mechanical wear). However it appears that additives and the presence of intergranular glassy films can apparently strengthen the grain boundaries, and therefore reduce this type of wear mechanism. For sub-micron grain sizes, wear occurs by a tribochemical mechanism and the wet erosive wear rate is expected to be approximately constant as it effectively depends on a solution of alumina in water under load. The wear data in Tables 1 and 2 are summarized graphically in Fig. 1 as a function of grain size and this data has been superimposed on the basic wear rate curve for pure alumina as a function of grain size first reported in Ref. 8. Generally it can be seen the additive liquid phase sintered (lps) alumina samples show a lower wear rate than a corresponding sample of pure alumina of the same mean grain size. Furthermore it is clear that the data for the lps additive samples also exhibits a dependence on grain size indicating that the dominant factor determining wear rate in these materials is indeed alumina grain size. However there are significant departures of this data from a smooth function and this presumably suggests that there is a second factor controlling wear rate which is clearly additive composition, or some property dependent on composition. Assuming that this factor is multiplicative (rather than additive or subtractive) which implies that the two factors (grain size and additive composition) are *inter-dependant*, then Fig. 2 displays the wear reduction factor for the individual lps additive samples (i.e. the fractional difference in wear rate between the sample in question and an alumina of the same median grain) as a function of calcia/silica molar additive ratio (here we confine ourselves to solely calcia/silica additions). Ignoring the point for the CS5 sample ($CaO:SiO_2 = 0.2$) which has a sub-micron grain size and should therefore wear by a tribochemical mechanism—thus giving a wear rate similar to a pure sub-micron alumina, Fig. 2 indicates that overall the addition of sintering additives improve the wear properties of alumina. The improvement in wear is most marked for silica-rich additions and the effect decreases as the level of calcia increases; there is also a suggestion of a minimum wear rate for small levels of calcia additions.

Molecular dynamics simulations of simple two grain boundaries in alumina have revealed that silicate intergranular films can, in principle, accommodate metal cations such as calcium or magnesium within a cage-like structure formed at the interfaces with the alumina grains.[9] Subsequent simulations of calcium silicate intergranular films[10,11] have suggested that for concentrations of up to 12 at.%, calcium cations prefer to segregate to these cage-like structures where they lower the glass/grain interfacial energy and promote ordering of the interfaces. Interestingly fracture simulations of

Table 1
Median grain sizes and wear rates for different amounts of sintering additives

Additive composition	Median grain size (μm)	Wear rate (wet erosion) (nm/s)	Literature
No additive	3.4±2.6	42±2.0	Ref. 5
10 wt.% (SiO_2)	2.87	18.5±0.8	Ref. 7
10 wt.% (10 SiO_2; 1CaO)	2.53	14.4±0.8	Ref. 8
10 wt.% (3 SiO_2: 1CaO)	2.04	17.1±0.8	Ref. 7
10 wt.% (1 SiO_2: 1CaO)	2.72	34.2±0.8	Ref. 7
0.5wt.%(1 SiO_2: 1MgO)	2.10±1.1	18.1±0.1	Ref. 5
1 wt.% (1 SiO_2: 1MgO)	2.00±0.9	13.5±0.7	Ref. 5
5 wt.% (1 SiO_2: 1MgO)	1.90±1	10.1±0.8	Ref. 5
10 wt.% (1 SiO_2: 1MgO)	1.80±1	9.6±0.4	Ref. 5

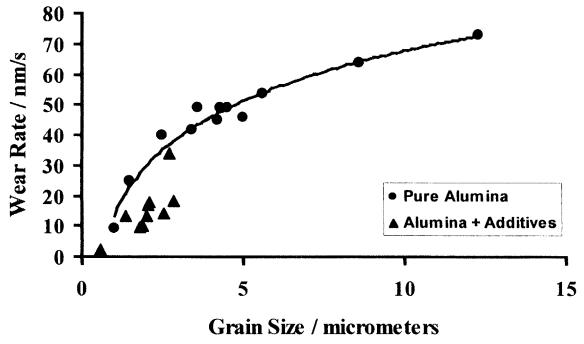

Fig. 1. Wear rate as a function of grain size.

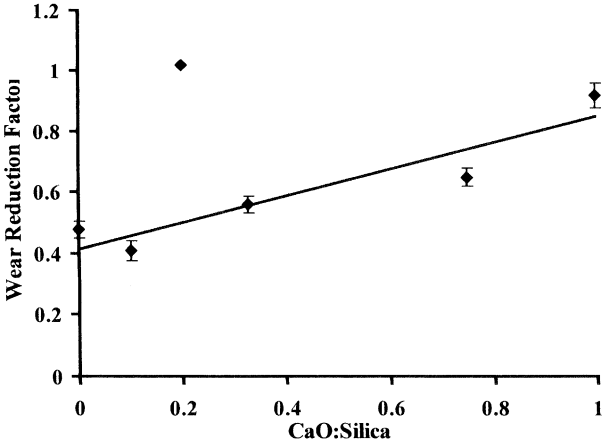

Fig. 2. Wear reduction factor as a function of additive composition.

these model interfaces revealed that, for low levels of calcia addition, fracture occurred only at the glassy film/alumina grain interface plane. Further increasing the calcia content disrupts the siloxane bonding within the intergranular film itself, enabling fracture through both the glass/grain interface and through the film interior so leading to a corresponding decrease in the overall fracture strength. Generally the presence of Ca lowers the interface energy of the grain boundaries and, if the intergranular silicate film has a calcia concentration of at least 30% and a thickness of at least 1.5 nm, this is predicted to give negative interfacial energies which would be expected to trigger abnormal grain growth during sintering.[10]

The aim of this work is to reveal the micro- and nanostructural differences between two polycrystalline aluminas hot pressed in the presence of 5 wt.% liquid phase-forming sintering additives of composition xCaO.ySiO$_2$ where $x=1$ and $y=1.33$ or $y=5$ respectively. These materials exhibited marked differences in mechanical properties, in particular, the performance under wet erosive conditions exhibited an order of magnitude reduction in wear rate for the material with the higher silica additive content.

Table 2
Properties of the examined samples

	CS5 specimen	CSp specimen
Additive composition	$CaO.5SiO_2$	$CaO.1.33SiO_2$
Medium grain size (μm)	0.56±0.05	1.36±0.05
Wear rate (nm/s)	2.1±0.2 with evidence of tribochemical wear mechanism.	13.4±0.7 with evidence of grain pull-out wear mechanism.
HV10 (GPa)	16.6±0.3	14.8±0.3
K_{IC} (MPa m$^{1/2}$)	2.4±0.2	2.9±0.2
Grain boundary	Amorphous film (~0.5 nm) of composition CaO:SiO_2 atomic ratio of between 1:11 and 25.5	Amorphous film (0.7–0.8 nm) of composition CaO:SiO_2 atomic ratio of between 1:1 and 3 (average 1.8)
Triple pocket glassy phase	Composition in mullite phase field (0–1 CaO:1.7–3.9SiO_2:Al_2O_3)	Composition in mullite phase field (CaO:2.3–9.5SiO_2:1.6–8.4Al_2O_3) average: (CaO:5.4SiO_2:3.9Al_2O_3)
Crystallized phase	Anorthite with composition in mullite phase field (CaO:4–6SiO_2:7–9Al_2O_3)	Gehlenite with composition on intersection between anorthite and gehlenite (CaO:1.1SiO_2:1.1Al_2O_3)
Residual stresses manifestation	Only a few dislocations observed	Many stress dislocations observed
Residual fluctuating local stress (MPa)	444±100	459±110
Mean residual compressive stress (MPa)	304±70	110±30

HV10-vickers hardness (10 N applied pressure), K_{IC}—fracture toughness, R_w—wet erosion rate.

2. Experimental

The alumina powders containing sintering additives (CaO and SiO_2) were prepared by ball milling a mix of Al_2O_3 powder (Martoxid CS400M, Martinswerke GmbH, Germany—mean particle size 400 nm) in isopropyl alcohol together with calcium nitrate $Ca(NO_3)_2.4H_2O$ (AnalaR grade, BDH Ltd., Poole, UK), and Tetraethylorthosilicate (TEOS), (AnalaR grade, BDH Ltd., Poole, UK) in a polyethylene jar. The amounts of additive components were adjusted to be equivalent to 5 wt.% of calcium silicate with $CaO:SiO_2$ molar ratios 1:1.33 (CSp-composition which is near to the local peritectic point in the $CaO–SiO_2–A1_2O_3$ ternary phase diagram) and 1:5 (CS5). After 2 h of homogenisation, an aqueous solution of ammonium hydroxide (10 wt.%) was added in order to precipitate calcium hydroxide, and to hydrolyze the TEOS. A further 1 h mixing at room temperature was allowed in order to finish the hydrolysis and then the suspension was dried under an infrared lamp. The dry powder was calcined for 30 mm at 750 °C and passed through a 100 μm mesh nylon sieve to provide a reasonably free flowing powder. This powder was hot-pressed for 10 min at 1450 °C at a pressure of 20 MPa.

For SEM examination, sintered specimens were sliced, polished, and thermally etched (1400 °C for 30 min), or alternatively in some cases chemically etched using boiling phosphoric acid, to reveal the grain boundaries. Finally, the samples were carbon coated to achieve an electrically conductive surface so as to avoid charging. Samples were examined in a CamScan IV SEM (Cambridge instruments, Cambridge, UK) and, to determine the median grain sizes, measurements were made from digital micrographs using Kontron, KS 400 standard image analysis software.

For TEM examination sintered specimens were core drilled and sliced to prepare 3 mm diameter discs of 500 μm thickness. The discs were further ground, polished, dimpled and then ion-milled (Gatan Precision Ion Polishing System model 691—low angle ion beam thinner) until electron beam transparent. The thin specimens were coated with an ultrathin conducting, amorphous carbon layer and examined using a transmission electron microscope (Philips CM200 FEG TEM) fitted with a scanning (STEM) unit, ultra thin window EDX detector (Oxford Instruments UTW ISIS EDX) and PEELS [Gatan Imaging Filter (GIF 200)].

For wear rate measurement only materials with bulk density greater than 98% of theoretical were used for further studies to avoid possible effects of porosity on wear rate. Discs with diameter 25 mm were weighed to ± 0.1 mg (w_1) and worn under carefully standardized conditions in an abrasive slurry consisting of 750 g fused alumina grit (Morganite 954 grog, Morganite Ceramics Ltd, Neston, UK) in 250 cm^3 distilled water. The grit consisted of approximately equiaxed angular particles with diameter between 0.5 and 1 mm. The hardness of the grit particles was not measured. The grit was used for a maximum of two measurements as its effectiveness as a wearing agent decreased significantly after approximately 14 h of testing due to rounding of grit particles. The disc was clamped horizontally in a specially designed cylindrical polyurethane block so as to expose approximately one half of the disc surface. The block was attached to the shaft of an attritor mill, and rotated at 500 r.p.m., giving an effective alumina disc perimeter velocity of 1.9 m s^{-1}. The wearing surface area (A) was assumed to be one quarter of the area of the disc peripheral rim. Experience had shown that the disc faces, although of higher area, wore very little. The final disc weight (w_2) was measured to ± 0.1 mg, and the weight losses occurring between the standard times of 2 h and 6 h were used to calculate a wear rate (R_w) from:

$$R_w = \frac{1}{A} \cdot \frac{w_1 - w_2}{\rho(t_2 - t_1)}$$

The times used were chosen in order to eliminate uncertainties caused by initial defects in disc surface finish, and the more significant wear of the grit particles which occurred at longer times. It had been shown that over this time interval R_w was independent of time.[12] Each disc could be used for two wear tests, and wear values reported below are the means of at least two determinations. Full details of the equipment and experimental procedures are given elsewhere.[13]

The polished specimens were indented by a Vickers indenter at 1 and 10 kg in order to evaluate the hardness [HV10 (GPa)] and fracture toughness [K_{IC} (MPa $m^{1/2}$)], respectively.[14] The fracture toughness was calculated from the length of the cracks emanating from the corners of the Vickers indentation impression by the method described by Anstis.[15]

Measurements of the residual fluctuating local stress and mean residual tensile stress[13] were performed using a Raman optical microprobe (Renishaw model 2000) and an incident radiation from a He/Ne laser with a photon wavelength of 633 nm. The incident beam was focussed on the polished surfaces of specimens through and Olympus microscope, with an objective magnification of ×50, corresponding to a laser spot diameter of about 3 μm. Then, Cr^{3+} photo-luminescence spectra, comprising the R1 and R2 luminescence lines, were recorded through a CCD array where each pixel covers a frequency range of about 1 cm^{-1}. Three measurements were carried out at randomly selected locations on each specimen. An air conditioning unit was used to maintain the room temperature at 20 °C±0.1 °C since the luminescence lines have a temperature dependence of 0.15 cm^{-1} K^{-1}. The spectrometer was calibrated before and after each experiment by taking a spectrum from an

unstrained sapphire crystal. The spectra from the sapphire crystal were also used as reference to determine the changes in the shape and position of the spectra obtained from the specimens. Curve fitting software (PeakFit v4) was used to determine the centre, full width at half height (FWHM), area and intensity of the R1 and R2 luminescence lines using a Gaussian-Lorentzian type fitting equation. The error of the fit was minimised by repeating the curve fitting procedure to yield an r^2 coefficient of determination greater than 0.999 ($0 < r^2 < 1$ and an r^2 of 1.0 indicates perfect fit) and a standard error of fit less than 0.1% of the value of each peak parameter considered. The characteristic frequencies of the two luminescence lines R_1 (at 1369 cm^{-1}) and R_2 (at 1397 cm^{-1}) are sensitive to lattice strain, and the piezoelectric coefficients are known. However, there is in general no simple relationship between the frequency shift ($\Delta\nu$) and stress (σ), because the frequency shift depends on the stress state. This technique has successfully been used to measure the mean residual stress in polycrystalline alumina as a function of grain size. In the case of residual stresses in alumina arising from anisotropic thermal contraction, results have been analyzed in terms of a residual mean compressive stress (σ_a) in the basal plane of each alumina crystal, and a mean tensile stress parallel to the c-axis in each crystal (σ_c). The two mean stresses are linked by the equation:

$$2\langle\sigma_a\rangle + \langle\sigma_c\rangle = 0$$

where chevron brackets denote average values. These stresses give rise to a frequency shift of the luminescence lines given by:

$$\langle\Delta\nu\rangle = \langle\sigma_c\rangle(\Pi_c - \Pi_a)$$

For the R, and R_2 lines Π_a and Π_b are 3.1 and 1.5 cm^{-1} GPa^{-1} ,[16] and so $<\Delta\nu>$ (expressed in units of cm^{-1}) $= -1.6 < \sigma_c >$ (units of GPa). For the R_2 lines the corresponding sensitivity factor is -0.57 cm^{-1} GPa^{-1}. The luminescence lines can be broadened by several effects, such as temperature, shear stress, and normal stress. The width of the luminescence line is characterized by the full width at half maximum ($f_{0.5}$) and the standard deviation in frequency is equal to $\{f_{0.5}/2.355\}$. The sensitivity to these parameters has been determined by He and Clarke[16] and it has been established that the effects of uniform stress are small (typically 0.3 cm^{-1} GPa^{-1}). If the stresses are not spatially uniform in the analyzed volume there is additional broadening of the luminescence lines with significantly greater sensitivity to stress differences. The non-uniform stresses can be spatially varying macroscopic stresses, or microscopic local stresses arising from defects such as dislocations and grain boundary heterogeneities. The additional line broadening is characterized by the mean square deviation in the frequency of the stressed material, compared with the mean square deviation of an unstressed crystal.[16] For the thermal contraction anisotropy stresses, the relationship between the frequency broadening and the mean square deviation in stress is given as:

$$\langle\Delta\nu^2\rangle = (4\Pi_a^2 + \Pi_c^2)\langle\sigma^2\rangle$$

Thus the standard deviations are related by (for the R_1 line):

$$\sqrt{\langle\Delta\nu^2\rangle} = 6.25\,(cm^{-1}\,GPa^{-1})\sqrt{\langle\sigma^2\rangle}$$

The factor for the R_2 line is 5.87 cm^{-1} GPa^{-1}. For microstresses the stress state is unknown, but on the assumption that the stresses are hydrostatic the proportionality constants are 7.59 cm^{-1} GPa^{-1} for the R_1 line and 7.61 cm^{-1} GPa^{-1} for the R_2 line. Because the stress state is uncertain we have taken average values of 6.9 cm^{-1} GPa^{-1} (R_1) and 6.7 cm^{-1} GPa^{-1} (R_2) for the coefficients relating peak width to stress variation.

3. Results

A summary of experimental results for the CS5 and CSp specimens is provided in Table 2. SEM images (Fig. 3) revealed considerable differences in microstructure between the two materials: the CS5 sample consisted of mainly equiaxed alumina grains with a median grain size of around 0.5 μm, whereas the CSp sample exhibited elongated alumina grains with an equivalent median grain size larger than 1 μm. It is interesting to note that thermal etching resulted in some grain and glassy phase pull-out in the CSp specimen, whereas the surface of the CS5 specimen was less affected by the process of thermal etching. We believe this is linked to the evidence for large stresses in sample CSp observed by TEM which are discussed below.

TEM of the specimens revealed a number of distinct findings. Firstly, the representative micrograph of the CS5 sample (Fig. 4a) shows a microstructure showing little evidence for strain or dislocation formation, whereas the micrograph of the CSp specimen (Fig. 4c) exhibits contrast consistent with the presence of considerable strains and evidence that associated stresses have been relaxed through formation of dislocation and microcracks arrays.

Secondly, in both samples TEM provided evidence for the formation of secondary crystalline phases at large volume triple junctions, where presumably the liquid has crystallised during processing or cooling. This was not observed in intergranular films at two grain

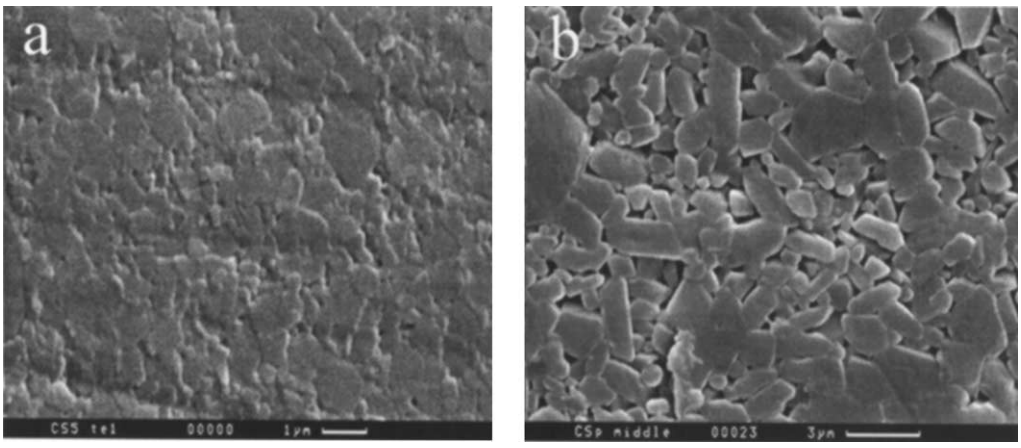

Fig. 3. SEM micrographs of (a) CS5 and (b) CSp specimens.

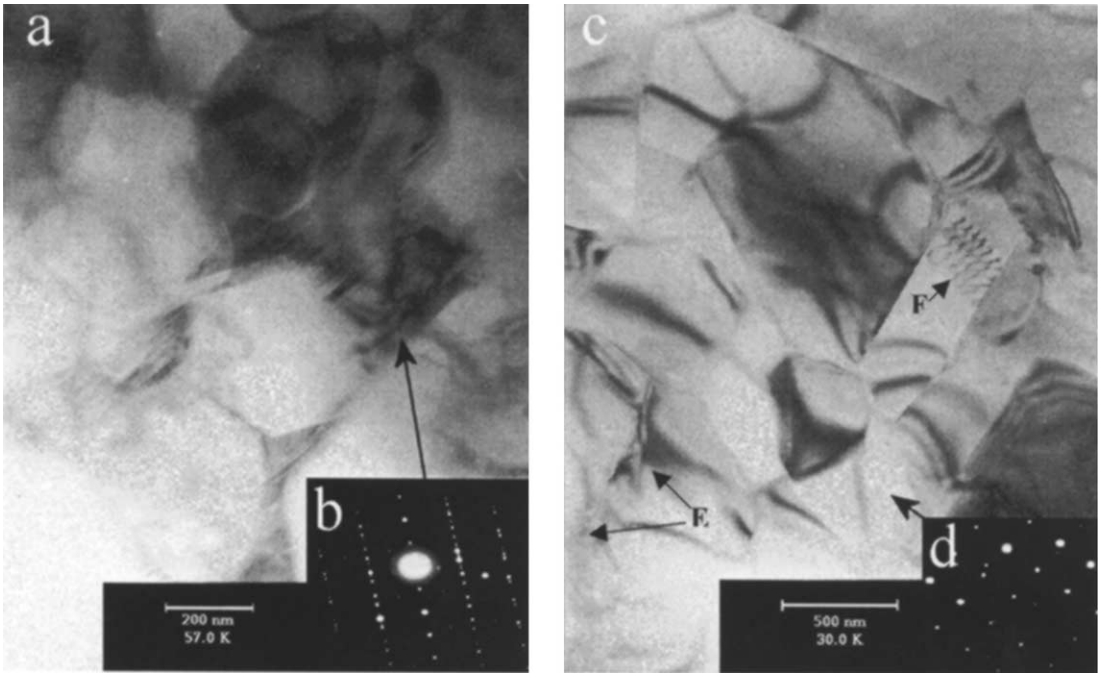

Fig. 4. (a) TEM bright field micrographs and (b) electron diffraction patterns of crystallized phase (anorthite) in CS5 specimen and (c) TEM bright field micrographs and (d) electron diffraction patterns of crystallized phase (gehienite) in CSp specimen. Note the diffraction camera lengths are not the same in (b) and (d). Microcracks (E) and fringes (F) in CSp specimen are a sign of heavily stressed material.

junctions presumably due to the restricted volume and the unfavourable strain energy terms involved during nucleation. Secondary crystallization was considerably more evident in the CS5 specimen (Fig. 4a), where in the bright field TEM image this was observed to result in heavily twinned crystals; selected area electron diffraction patterns (Fig. 4b) from this secondary crystalline phase could be indexed to the anorthite structure which is commonly known to exhibit such twins. Although the nominal composition of anorthite is $CaO.2SiO_2.Al_2O_3$, STEM/EDX elemental analysis suggested that the composition of this crystalline phase lay in the mullite phase field of the ternary phase diagram (Fig. 5); the unexpectedly low calcium content may be due to the use of intense focused electron probes which was noted to cause some migration of Ca away from the analysis area or, alternatively, the competition between crystallization of this secondary phase and the driving force for segregation of Ca to the surface of alumina grains which has been observed before[4,7] and was also detected in this study when analyzing the interfaces between a grain and the triple pocket glass. STEM/EDX elemental mapping of the CSp specimen revealed that any secondary crystalline phases, which were not seemingly as widespread as in the CS5 specimen, tended to be concentrated in larger pockets and contained a larger concentration of

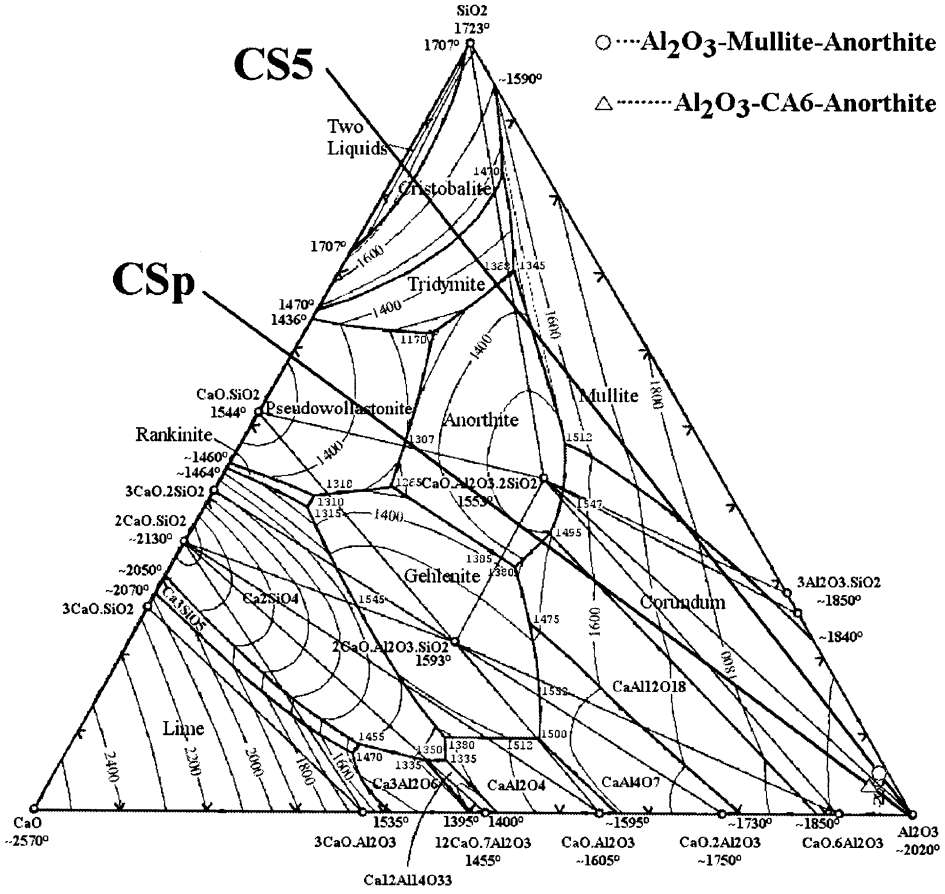

Fig. 5. Ternary phase diagram of system $CaO–SiO_2–Al_2O_3$.

calcium than in the corresponding secondary crystalline phases within the CS5 specimen, this being presumably related to the larger proportion of calcia in sintering additives (Table 2). Selected area electron diffraction patterns of crystallized phases in the CSp specimen (Fig. 4d) revealed lattice spacings that were consistent with that of gehlenite (nominally of composition $2CaO.SiO_2.Al_2O_3$).

STEM/EDX elemental mapping of both the CS5 and CSp specimens showed the concentration of calcia and silica in large triple pockets (Figs. 6 and 7 respectively). Although the triple pocket glasses varied in composition somewhat within a given specimen microstructure, the average glass compositions of both specimens lay nominally within the mullite phase field, however the glass in CSp specimen contained considerably more calcia (relative to sample CS5) (Table 2) as expected from the additive molar ratios. The most notable finding was the extremely differing compositions of the grain boundary intergranular glass film and the triple pocket glass in the CSp sample. In the CSp sample high resolution imaging revealed limited evidence for an amorphous grain boundary film of width between 0.7 and 0.8 nm (Fig. 8). STEM/EDX analyses using "letterbox" scans of width approximately 10 nm suggested that this intergranular film in CSp contained a significant proportion of calcia, which suggested an anorthite-like composition (assuming alumina was present as well). Note the analysis of the aluminium content of the intergranular glass films is complicated by the presence of the neighbouring alumina grains which are undoubtedly included in the analysis volume, hence, with the attainable spatial resolution for analysis in the FEGTEM plus the beam broadening effects due to sample thickness, it is really only meaningful to extract calcia:silica ratios from the present STEM/EDX results.

In the CS5 sample, high resolution imaging revealed an amorphous film at two grain boundaries less than half a nanometre in thickness (Fig. 9). STEM/EDX reduced area "letterbox" scan analysis suggested that the intergranular film contained a glass of similar composition to that in the triple pockets, although some intergranular films appeared very deficient in calcia. Assuming alumina was present as well, overall the average composition of the intergranular glassy phase in CS5 suggests a nominal composition lying in the mullite phase field according to the ternary phase diagram shown in Fig. 5. Besides

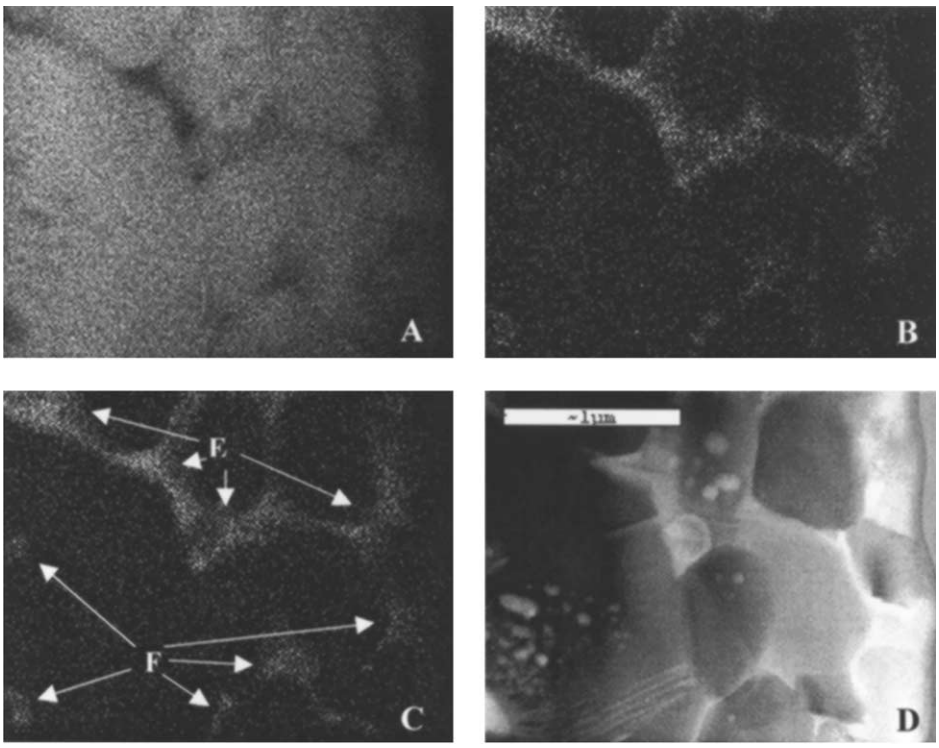

Fig. 6. EDX elemental analysis of CS5 specimen: (A) Al Kα map, (B) Ca Kα map, (C) Si Kα map, (D) STEM dark field image. Note the anorthite phase (E) contains a larger amount of calcium than glassy phase (F).

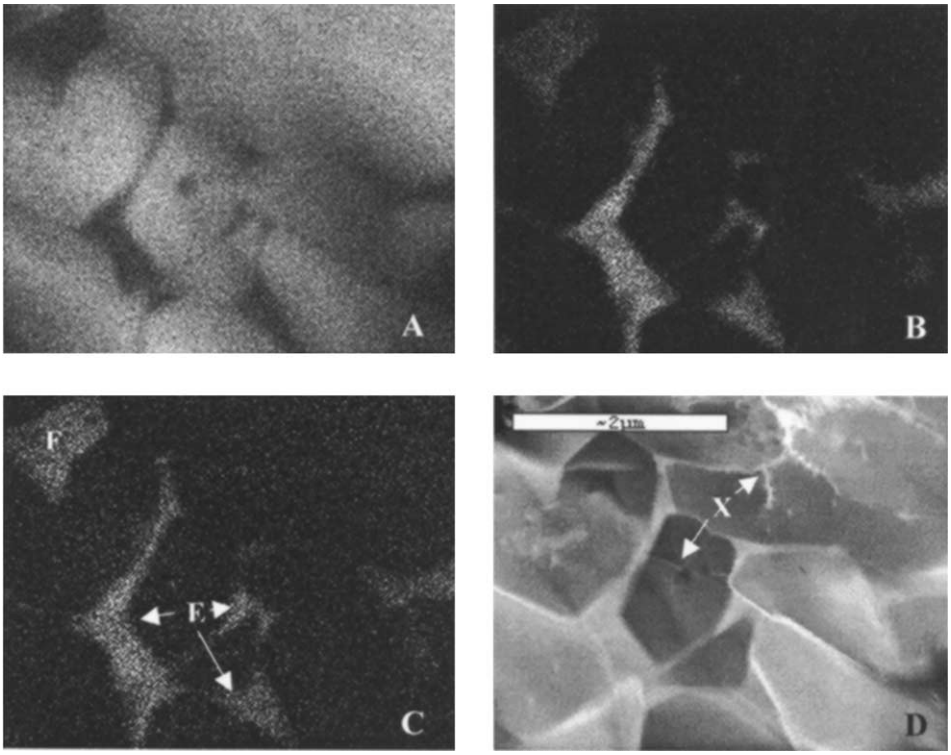

Fig. 7. EDX elemental analysis of CSp specimen: (A) Al Kα map, (B) Ca Kα map, (C) Si Kα map, (D) STEM dark field image. Note the gehlenite phase (F) contains a larger amount of calcium than glassy phase (F) and there is visible effect of stress (X)—microcracks and dislocations.

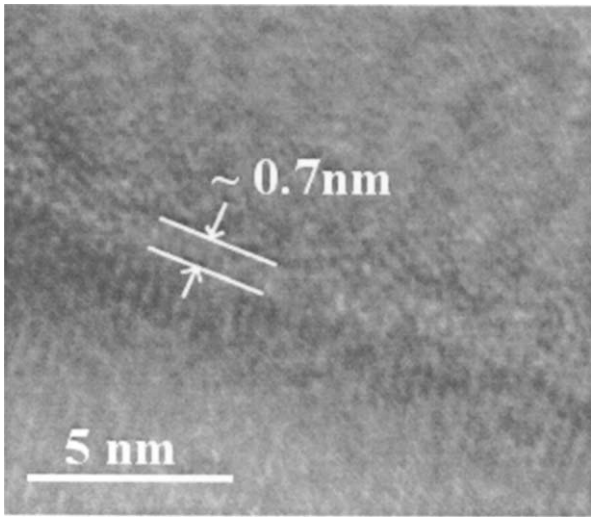

Fig. 8. High resolution image of a grain boundary in the CSp specimen.

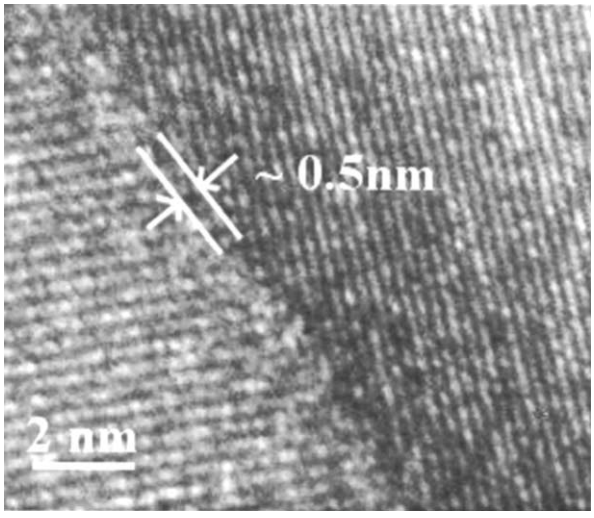

Fig. 9. High resolution image of a grain boundary in the CS5 specimen.

preferential loss of Ca from the analysis area during electron beam irradiation, presumably one reason for the deficiency in calcia in the intergranular film in CS5 may be related to the extensive crystallization of (albeit Ca-poor) anorthite.

4. Discussion

SEM of the CSp sample revealed a bigger surface deterioration following thermal etching than was observed in the CS5 sample. A similar behaviour has been found in previous studies where chemical etching was employed.[5] It is possible that this behaviour can be linked to the chemistry of the intergranular and secondary crystalline phases and also to the thermal shock applied during etching on the heavily defective microstructure of the CSp specimen.

The main goal of this present work was to ascertain the reason why the wear resistance is so different in these two specimens. One clue was provided by simple grain size analysis, the CS5 specimen has median grain size more than 2 times lower than the CSp specimen (Table 2); furthermore the grain aspect ratio is increased for the CSp specimen. Considering the fact that the same starting powders were employed for each specimen, together with equivalent conditions during sintering, the only remaining variables that could affect grain growth are the composition(s) of glassy phase(s) formed by the sintering additives and the alumina. Thus the higher level of calcia in the sintering additives in the CSp sample appears to promote the abnormal growth of elongated alumina grains which is consistent with our previous studies[4,7] and those of many other authors—for example in publications.[17–20] This presumably arises due the preferential adsorption of calcium ions onto certain crystallographic planes of the alumina grain surfaces, most probably the prism planes (which are {10-10} and {11-20}) as has been observed for lanthanum ions in silicon nitride.[21] It is presumably calcium which is facilitating the dissolution of alumina into the silicate glass, ultimately forming a calcium aluminosilicate glass which permits solution–precipitation processes necessary for liquid phase sintering. Low levels of calcium in the glass are expected to lower the interfacial energy between the alumina grain and the glass,[9–11] whereas a glassy phase richer in calcium (as observed in the triple pockets and intergranular films in the CSp sample relative to the CS5 sample) may lead to negative interfacial energies between the grains and the glassy phase which may result in abnormal alumina grain growth in that direction.

Previous work[5,7,8] has shown that ceramic materials with smaller median grain size show lower wear rates. This is summarized in the graph shown in Fig. 1 and arises from a number of factors detailed below:

1. When grain pull-out occurs, as in mechanical wear, a smaller volume of material is removed as grain size decreases;
2. The glass matrix is likely to have a much lower modulus of elasticity (Young's modulus) than the alumina grain, therefore some relaxation of the stresses generated by the anisotropic thermal expansion of alumina crystals can occur, mainly at higher temperatures ($T > T_g$) due to viscous flow. This relaxation should occur more easily for smaller grains rather than larger grains due to their higher surface area to volume ratio. Both the elastic modulus and the glass viscosity are expected to be an inherent function of glass composition—it is expected that both the elastic

modulus will and the viscosity will decrease as calcia content of the glass increases.[22]

3. The energy needed for crack progression during transgranular fracture is the same for large and small crystals. This implies that more energy must be dissipated for the same crack length in smaller grain materials, because the energy required scales with the number of cracked crystals, which will be correspondingly higher in a small grained material.

However, we believe that the rate of mechanical wear, dominant in supra-micron alumina grain size materials, will also affected by the chemical composition and the overall amount of sintering additives. This arises since the intergranular glass may affect both the level of residual stresses and possibly the relaxation of intrinsic residual stresses (due to the inherent anisotropy of alumina) in the polycrystalline sample, furthermore intergranular fracture may also become an important mechanism during the process of grain pull-out and this is expected to be highly dependent on the intergranular glass chemistry.

Molecular dynamics simulations of silicate grain boundary films in alumina[9] predict the existence of cage-like structures at the interface between the alumina grain and the glassy film. If calcium is present in the grain boundary film below 12 molar percent this is predicted to lead to the accommodation of calcium cations within this cages,[10] which will result in a lowering of the interfacial energy and an increase in the work required for intergranular crack propagation and hence grain pull-out. It appears that this condition is indeed satisfied in the CS5 specimen and the low levels of calcia in the triple pockets and intergranular films found in this sample may be related to the extensive crystallization of the secondary anorthite phase observed within large volume triple pockets which may provide a "sink" for excess calcia within the glass. Additionally this crystallization mechanism may be the reason that the triple pocket and grain boundary glasses in the CS5 specimen are of a more similar composition, in terms of their calcia:silica ratio, relative to those in the CSp specimen. However, the higher levels of calcia found in the grain boundary intergranular films in the CSp specimen (Table 2), where there is correspondingly less evidence for a secondary crystalline phase acting as a "sink", would be expected to lower the work required for intergranular fracture as the excess calcia in the glass film (above that required to saturate the interface with alumina grain) is expected to become incorporated in the silicate film network and act as a network modifier significantly changing the glass properties. A further consequence of the absence of extensive secondary crystallization in CSp may also explain why the chemistries of the triple pocket and grain boundary glasses in the CSp sample are inherently different as has been found in a CS sample (calcia:silica additive molar ratio equal to 1).[4,7]

It is possible that the fundamental difference in the chemistry and microstructure between the two samples may be understood by consideration of the ternary phase diagram shown in Fig. 5, where the nominal composition of the CS5 (circle) and the CSp (triangle) sample systems are both marked. Initially we have a situation where alumina grains are in contact with a surface layer of calcium silicate glass of composition either CS5 or CSp. As the temperature is raised, alumina progressively dissolves in the calcium silicate and the glass composition will move along one of the two tie lines marked in Fig. 5, e.g. CS5-alumina or CSp-alumina. For both systems at the sintering temperature of 1450 °C, we expect the initial glass composition to lie within the anorthite phase field. For the CSp sample we expect that the phases in equilibrium with alumina will be anorthite and calcium hexaluminate, while for the CS5 sample alumina is expected to coexist with anorthite and mullite. However it is important to realise that the sintering temperature is only 1450 °C which may make crystallization difficult and it is possible that we have the development of glassy phases with appropriate composition instead; this being said the most likely candidates for secondary crystallization would be expected to be anorthite and possibly gehlenite.

An additional factor which should have big influence on the wear resistance of these two materials are the local residual tensile stresses resulting from the thermal expansion mismatch between the anisotropic alumina grains[24] (Table 3) themselves as well as between alumina, the glassy phases and the crystallized phases. Generally it appears that a calcium aluminosilicate glass has a lower thermal expansion coefficient than that of alumina, although increasing calcium content in the glass reduces these differences;[25] the secondary crystalline phases such as anorthite have a lower thermal expansion coefficient as well, however, gehlenite is reported to possess a thermal expansion coefficient similar to that of alumina (Table 3). These local stresses may strengthen grain boundaries via the formation of compressive hoop stresses, particularly for silicate-rich

Table 3
Volumetric {linear} thermal expansion coefficients of crystalline phases found in CS5 and CSp specimens

Mineral	α(volumetric) {α(linear)} $\times 10^6$ K^{-1} [a]	α(linear) $\times 10^6$ K^{-1} [b]
Alumina (corundum)	26.8 {8.93 (polycrystalline)}	*a*-axis 8.6 *c*-axis 9.6
Anorthite	16 {5.33}	
Gehlenite	25 {8.33}	

[a] Ref. 23.
[b] Ref. 24.

films where the thermal expansion mismatch is largest, and this therefore leads to grain boundary clamping which is presumably the case in the CS5 specimen where the intergranular films are more calcia-deficient.

In the CSp specimen the existence of dislocations and microcracks throughout the alumina grains was observed. Presumably this is the reason for the lower local residual tensile stresses observed as lower shifts of the R1 line in Cr^{3+} photoluminescence spectra (Table 2). These strains, dislocations and microcracks most likely arise from the substantially different compositions observed between the glass at triple junctions and two-grain junctions in this sample, whereas conversely the CS5 microstructure has a more homogeneous glass composition. Such differing glass compositions may lead to stresses due to thermal expansion mismatches, and furthermore the higher calcia content in the grain boundary glass in CSp may result in a different elastic modulus of the intergranular glass thus changing the likelihood of effective stress relaxation processes between alumina grains. The lower wear resistance of the C Sp specimen may therefore also be a result of the damaged microstructure which will allow crack advance to occur more easily.

5. Conclusion

This study has attempted to ascertain the microstructural reasons for the difference in wear rates between the two polycrystalline aluminas processed and sintered under identical conditions but with differing molar ratios of calcia and silica sintering additives. The most probable conclusion is that grain size together with the mechanical and thermal properties of the intergranular and triple pocket glass and also any secondary crystalline phases are the main factors controlling the wear rate; these factors are clearly interdependant on one another. The latter factor can have either a strengthening effect—grain boundary clamping (the low calcia CS5 specimen) or a weakening effect—grain boundary wedging accompanied by the generation of the microcracks and dislocations (the high calcia CSp specimen). The CS5 specimen was found to be fine grained without signs of damaged microstructure, whereas in the CSp sample we observed a bigger grain size together with a vastly damaged structure, which resulted in large scale grain pull out during wet erosive wear process and hence a bigger wear rate in comparison to the CS5 specimen.

Acknowledgements

The support of this work by the Marie Curie Fellowship (for P.S.) under the contract number HPMF-CT-2002-01878, National Slovak Grant Agency under the contract No. 2/3101/23, the NATO Science for Peace Programme, the EPSRC (for a studentship to F.L.) and by the project No. 97 41 22, from the Alexander von Humboldt Foundation is gratefully acknowledged. The authors wish to thank Prof. Alan Atkinson at Imperial College, UK for the residual stress measurements.

References

1. Tomsia, A. P. and Glaeser, A. M., eds., *Ceramic Microstructures '96*. Plenum Press, New York, 1998.
2. Gu, H., Cannon, R. M. and Ruhle, M., *J. Mater. Res*., 1998, **13**, 376.
3. Chiang, Y. M., Wang, H. and Lee, J. R., *J. Microscopy*, 1998, **191**, 275.
4. Brydson, R., Chen, S., Pan, X., Riley, F. L., Mime, S. J., Pan, X. and Ruhle, M., *J. Am. Ceram. Soc*., 1998, **81**(2), 369.
5. Galusek, D., Brydson, R., Twigg, P. C., Riley, F. L., Atkinson, A. and Zhang, Y., *J. Am. Ceram. Soc*., 2001, **84**(8), 1767.
6. Galusek, D., Twigg, P. C. and Riley, F. L., *Wear*, 1999, **233**, 588.
7. Brydson, R., Twigg, P. C., Loughran, F. and Riley, F. L., *J. Mater. Res*., 2001, **16**(3), 652.
8. Miranda-Martinez, M., Davidge, R. W. and Riley, F. L., *Wear*, 1994, **172**, 41.
9. Blonski, S. and Garofalini, S. H., *J. Phys. Chem*., 1996, **100**, 2201.
10. Blonski, S. and Garofalini, S. H., *J. Am. Ceram. Soc*., 1997, **80**(8), 1997.
11. Litton, D. A. and Garofalini, S. H., *J. Mater. Res*., 1999, **14**(4), 652.
12. Miranda-Martinez, M. *Wet Erosive Wear of Technical Ceramics*. PhD Thesis, University of Leeds, 1994.
13. Galusek, D., Riley, F. L., Atkinson, A., Zhang, Y. H. and Brydson, R., *Key Engineering Materials*, 1999, **175–176**, 189.
14. Galusek, D., Kido, L., Panek, Z., Lences, Z., Sajgalik, P. and Riley, F. L., *Key Engineering Materials*, 2002, **223**, 227.
15. Anstis, G. R., Chantikul, P., Lawn, B. R. and Marshall, D. B., *J. Am. Ceram. Soc*., 1981, **64**, 533.
16. He, J. and Clarke, D. R., *J. Am. Ceram. Soc*., 1995, **78**, 1347.
17. Jung, J. and Baik, S., *J. Am. Ceram. Soc*., 2003, **86**(4), 644.
18. Bae, S. I. and Baik, S., *J. Am. Ceram. Soc*., 1993, **76**(4), 1065.
19. Lee, S. H., Kim, D. Y. and Hwang, N. M., *J. Eur. Ceram. Soc*., 2002, **22**, 317.
20. Cook, R. F. and Schrott, A. G., *J. Am. Ceram. Soc*., 1988, **71**(1), 50.
21. Hoffman M. and Raphaelle S. Private communication at Engineering Ceramics 2003, Smolenice, Slovakia, 11–15 May, 2003.
22. Bansal, N. P. and Doremus, R. H., eds., *Handbook of Glass Properties*. Academic Press, 1986.
23. Gottchalk, M., *Eur. J. Mineral*., 1997, **9**, 175.
24. Rice, R. W. and Frieman, S. W., *J. Am. Ceram. Soc*., 1981, **64**, 350.
25. Galusek, D., Majling, J., Lichvar, P., Gersi, P. and Chromcikova, M. In *Proc. of the 15th Int. Conference on Thermal Analysis and Calorimetry TERMANAL*, September 2000, Stara Lesna, Slovak Republic.